RSC Advances

Electrochemical-driven water reduction and oxidation catalyzed by an iron(III) complex supported by 2,3-bis(2-hydroxybenzylideneimino)-2,3-butenedinitrile

Journal:	*RSC Advances*
Manuscript ID:	RA-ART-03-2015-005520.R2
Article Type:	Paper
Date Submitted by the Author:	01-May-2015
Complete List of Authors:	Zhan, Shuzhong; College of Chemistry ? Chemical Engineering, South China University of Technolog, ; Fu, Ling-Zhi; South China University of Technology, Zhou, Ling-Ling; South China University of Technology,

Journal Name

RSCPublishing

ARTICLE

Electrochemical-driven water reduction and oxidation catalyzed by an iron(III) complex supported by 2,3-bis(2-hydroxybenzylideneimino)-2,3-butenedinitrile

Cite this: DOI: 10.1039/x0xx00000x

Received 00th January 2012,
Accepted 00th January 2012

DOI: 10.1039/x0xx00000x

www.rsc.org/

Ling-Zhi Fu, Ling-Ling Zhou and Shu-Zhong Zhan*

One molecular electrocatalyst for both water reduction and oxidation, based on an iron(III) complex [FeLCl(H_2O)] **1**, is formed by the reaction of anhydrous $FeCl_3$ with a tetradentate ligand, 2,3-bis(2-hydroxybenzylideneimino)-2,3-butenedinitrile (H_2L). Its structure has been determined by X-ray diffraction. **1** elcetro-catalyzes hydrogen evolution both from acetic acid and water, with a turnover frequency (TOF) of 10.25 and 808.46 moles of hydrogen per mole of catalyst per hour at an overpotential of 893 mV (DMF) and 837 mV (pH 7.0), respectively. Water oxidation occurs at an overpotential of 677 mV to give O_2 with a TOF of ~0.849 s^{-1}.

Introduction

Water is the only waste-free electron-source substrate that could sustain the scale of the process required to supply our energy demands. Thus, splitting water into hydrogen and oxygen is one of the most attractive scenarios for sustainable energy production. [1,2] However, this electrochemical conversion stores 1.23 V and consists of the four electrons, four proton oxidation of water to oxygen and the reduction of the produced protons to hydrogen. One of the key challenges to water splitting is the development of efficient catalysts for water reduction and oxidation. In Nature, Fe-Ni and Fe-Fe hydrogenases produce H_2 in water at close to the thermodynamic potential of -0.41 V vs the normal hydrogen electrode (NHE) at pH 7.0. [3] However, enzymes are difficult to obtain in sufficient amounts to adapt for commercial applications and their stability is often limited outside of their native environment. [4] Many research groups, including ours, have tried to develop molecular catalysts by employing transition metals, and several complexes that contain nickel, [5] cobalt, [6-10] copper [11-14] and molybdenum [15-17] have been developed as electrocatalysts for the reduction of water to form H_2.

In other hand, the notable progress also has been made in homogeneous water oxidation catalysis with transition metal complexes, including cobalt, [18-20] copper [21,22] and iron. [23-28] However, there have been few complexes reported in the literature that can function efficiently as both water oxidation catalysts (WOCs) and water reduction catalysts (WRCs). This is attributed to that WOCs and WRCs require different types of ligands to support. Efficient WOCs generally are in the form of metal oxides [29] or with oxidation-resistant ligands, [30] while efficient WRCs prefer softer ligands to generate low-valent active intermediates that can reduce proton at low over-potentials, such as oxime ligand. [31] As an expanded work, [14,32] reported here is the synthesis and characterization of a water-soluble iron(III) complex, [FeLCl(H_2O)] **1**, as well as its electro-catalytic properties for water oxidation and reduction thereof.

Results and discussion

The reaction of $FeCl_3 \cdot 6H_2O$ with H_2L in the presence of NEt_3 affords an iron(III) complex, [LFeCl(H_2O)] **1** (Scheme 1), which is

soluble in water and common organic solvents, such as DMF and CH_3CN, *etc*. Electronic absorption spectrum of complex **1** shows multiple intense bands in the UV and visible regions (Fig. S1). The bands between 300 and 370 nm are due to LMCT (n–π*), and the band at 493 nm is attributed to the d–d transition. The UV/Vis spectrum of **1** in water shows one intense band at 302 nm from ligand π→π transition, and two peaks at 373 and 473 nm from a metal d–d transition (Fig. S2). And the UV/Vis spectra of **1** in buffered aqueous solutions (KH_2PO_4 + NaOH) from pH 4.5 to 11.5 exhibit similar peaks to those in water. When pH = 12.5, a new absorption peak at 402 nm appeared, suggesting that this complex decomposes to a new component under these conditions (Fig. S3). Therefore, we can explore its electrochemical properties in the pH range 4.5-11.5.

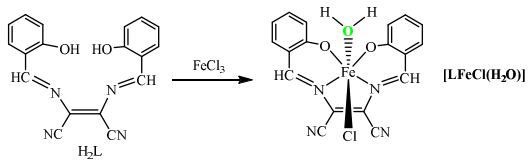

Scheme 1. Schematic representation of the synthesis of complex [LFeCl(H_2O)] **1**.

As shown in Fig. 1, the title complex consists of one Fe^{3+} ion, one L^{2-} ion, one Cl^- and one H_2O molecule. The iron atom is surrounded by two nitrogen atoms and two oxygen atoms from Schiff-base ligand ion (L^{2-}), one Cl^- and one oxygen atom from H_2O molecule. The average bond length of Fe-N is 2.129(15) Å. The Fe(1)–Cl(1) bond distance of 2.3098(6) Å in complex **1** is similar to that Fe–Cl bonds in iron(III) complexes possessing similar tetradentate ligands. [33] The distance between Fe and O from H_2O molecule (2.2086(13) Å) is longer than that of Fe-O(L^{2-}) (*av*, 1.8939 Å), suggesting that **1** is more soluble in water.

As shown in Fig. 2, the cyclic voltammogram of 3.17 mM complex **1** shows one reversible Fe^{III}/Fe^{II} couple at -0.08 V. Scanning to cathodic potential beyond the first reversible reduction reveals an quasi-reversible redox event at -0.84 V followed by another one quasi-reversible couple at -1.55 V. For comparison, CV of ligand was measured in a similar condition (Fig. S4). The second reduction wave of **1** at -0.84 V, being close to the second reduction of the free ligand, is assigned to the ligand. The third redox peak is assigned to the Fe^{II}/Fe^{I} couple. Scan rate analyses of voltammograms exhibit linear dependences in plots of current vs $v^{1/2}$ (Fig. S5), as expected for diffusional species at all observed redox events.

To determine possible electrocatalytic activity of this complex, cyclic voltammograms of complex **1** were recorded in the presence of acetic acid. Fig. 3 shows a systematic increase in i_{cat} observed near -1.41 V with increasing acetic acid concentration from 0.0 to 5.44 mM. This rise in current can be attributed to the catalytic generation of H_2 from acetic acid [11]. This clearly dictates that hydrogen evolution electrocatalyzed by **1** requires the reduction of Fe(II) to Fe(I).

To confirm that complex **1** was indeed responsible for the catalytic reaction, the free ligand, $FeCl_3$, and the mixture of the free ligand and $FeCl_3$ were each measured under identical conditions. As can be seen in Figs. S6-S7, the catalytic competency achieved with **1** is not matched by just ligand, $FeCl_3$, or the mixture of the free ligand and $FeCl_3$, nor can it be accomplished with the ligand bound to a redox-inactive metal. Thus, a combination of the iron ion and the ligand is essential for catalytic activity.

Further evidence for the electro-catalytic activity was obtained by bulk electrolysis of a DMF solution of complex **1** (5.80 μM) with acetic acid (5.44 mM) at variable applied potential using a glassy carbon plate electrode in a double-compartment cell. Fig. 4-a exhibits the charge of bulk electrolysis of complex **1** in the presence of acid. When the applied potential was -1.40 V versus $Ag/AgNO_3$, the maximum charge reached 25 mC during 2 min of electrolysis. A controlled-potential electrolysis (CPE) experiment under the same potential with a catalyst-free or ligand solution only gave a charge of 8 and 9 mC, respectively (Fig. 4-b), indicating that this complex does indeed serve as an effective hydrogen production catalyst under such conditions. According to *eq*. (1), [11] a TOF for the catalyst reaches a maximum of 10.25 moles of hydrogen per mole of catalyst per hour at an overpotential of 891 mV (Eq. S1 and Fig. S8).

$$TOF = \Delta C / (F*n_1*n_2*t) \qquad (1)$$

Where, Δ*C* is the charge from catalyst solution during CPE minus charge from solution without catalyst during CPE, F is Faraday's

constant, n_1 is the mol of electrons required to generate a mol of H_2, n_2 is the mol of catalyst in solution, t is duration of electrolysis.

To explore the electrochemical behavior of complex **1** in aqueous media, a much more attractive medium for the sustainable generation of hydrogen, CVs were measured in buffered solutions (KH_2PO_4 + NaOH). In pH 7.0 buffer, complex **1** shows one reversible Fe^{III}/Fe^{II} wave at -0.62 V (Fig. 5-inset) and one irreversible Fe^{II}/Fe^{I} wave at -1.58 V (Fig. 5), respectively. The redox wave at -1.58 V (Fe^{II}/Fe^{I}) is dependent of pH (Fig. S9), and the current response of the redox events at -1.58 V also varies linearly on the square root of the scan rate, which is an indicative of a diffusion-controlled process (Fig. S10).

From CPE experiment, when an applied potential was -1.45 V versus Ag/AgCl, the maximum charge was only 28 mC during 2 min of electrolysis in absence of complex **1** (Fig. 6-a). Under the same conditions, the charge reached 600 mC with addition of complex **1** during 2 min of electrolysis (Fig. 6-b), accompanying evolution of a gas (Fig. S11), which was confirmed as H_2 by gas chromatography. According to Fig. S12-a, ~3.9 mL of H_2 was produced over an electrolysis period of 1 h with a Faradaic efficiency of 96% for H_2 (Fig. S12-b). TOF for electrocatalytic hydrogen production by complex **1** is 808.46 moles of hydrogen per mole of catalyst per hour at an overpotential of 837.6 mV (pH 7.0) (Eq. S2 and Fig. 6-c), which is higher than that of a similar copper(II) complex [LCu] (457 moles of hydrogen per mole of catalyst per hour at an overpotential of 817 mV), [11] indicating that the iron(III) electrocatalyst is more active than the copper(II) species. A possible explanation could be that iron center in a square planar geometry is attacked by H^+ or H_2O more readily than the copper complex.

To explore the catalytic water oxidation by complex **1**, CVs were conducted in an aqueous solution and buffers (KH_2PO_4 + NaOH) at different pH values. At more positive potentials, two irreversible oxidation waves appear at 0.89 V and 1.40 V vs Ag/AgCl in a 0.10 M KNO_3 solution, corresponding to Fe^{IV}/Fe^{III} and Fe^{V}/Fe^{IV}, respectively (Fig. 7-a), with a greatly enhanced underlying current compared to the background. Fig. 7-b exhibits a systematic increase in i_{cat} with increasing pH from 7.0 to 11.8. Cyclic voltammogram of background in the absence of complex **1** exhibits no catalytic current at the potential of the couples of Fe^{IV}/Fe^{III} and Fe^{V}/Fe^{IV} (Fig. 7-a, black line), suggesting that water oxidation to O_2 occurs with complex **1**. [22] The current enhancement for the wave at $E_{p,a}$ = 0.89 V is consistent with catalytic water oxidation, with catalytic onset shift to more negative potentials (from 1.50 V to 0.78 V). The current enhancement for the wave at 1.18 V is also consistent with catalytic water oxidation with catalytic onset shift to more negative potentials (from 1.30 V to 0.95 V). On the basis of literature precedent [34] and above analyses, we propose the catalytic cycle depicted in Scheme 2 for the generation of O_2 from water mediated by **1**. In this mechanism, the product of the second oxidation would be the formally Fe^{IV} species, a high-oxidation Fe-oxo intermediate as sites for O-O coupling and water oxidation, as found in other complexes. [35,36] Analysis of the anodic scans of the redox couples at 0.89 V and 1.40 V as a function of scan rates (Fig. S13) both show a linear relation, consistent with adsorption of the molecules on the electrode surface.

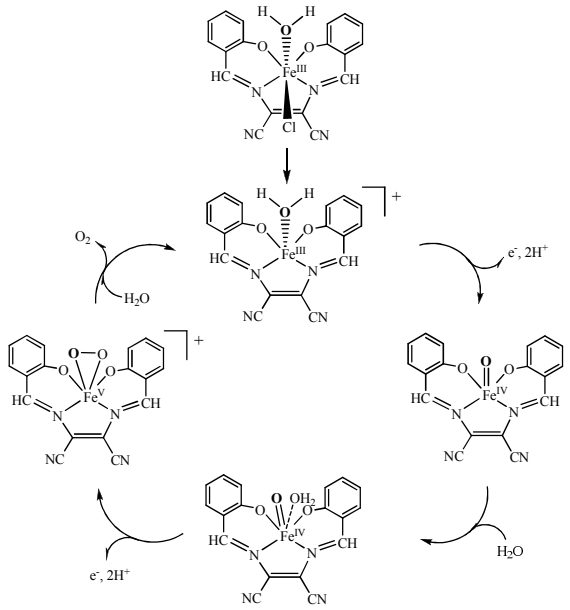

Scheme 2. Proposed mechanism for electrocatalytic water oxidation by [LFe(H_2O)Cl] **1**.

Evolution of O_2 as a product was investigated by controlled potential electrolysis on an ITO (1.32 cm^2) electrode with complex **1** in a 0.25 M buffer solution (pH 10.5). The background for oxygen formation at the applied potential in the absence of catalyst is only 28 mC during 2 min of electrolysis (Fig. 8-a). With addition of **1**, the amount of charge used in 2 min increases with increasing the applied potential (Fig. 8-b), accompanying the formation of a large amount of gas bubble. The evolved O_2 was analyzed by gas chromatography, Fig. 9-a, which gave ~28 μmol of O_2 over an electrolysis period of 5 h with a Faradaic efficiency of 93% for O_2 (Fig. 9-b).

This study stated clearly that **1** is capable of catalyzing the oxidation of water to O_2. According to *eq*. (2), [21] n_p is the number of electrons transferred in the noncatalytic wave, n_c is the mol of electrons required to generate a mol of O_2 and ν is the scan rate. From the slope of the plot of i_{cat}/i_d versus $\nu^{-1/2}$ (Fig. S14), we calculated k_{cat} for the catalyst reaching a maximum of 0.01 s^{-1} ($E_{p,a}$= 0.83 V, and Eq. S3), and 0.849 s^{-1} ($E_{p,a}$= 1.18 V, and Eq. S4), respectively, indicating that both couples Fe^{IV}/Fe^{III} and Fe^{V}/Fe^{IV} are devoted to water oxidation. This value (0.849 s^{-1}) is higher than some reported molecular water oxidation catalysts, [37-39] yet much lower than the recently reported iron based one. [40]

$$\frac{i_c}{i_p} = 0.359\frac{n_c}{n_p^{3/2}}\sqrt{k_{cat}/\upsilon} \qquad (2)$$

The low active catalyst for water oxidation is attributed to 1) The planar ligand, 2,3-bis(2-hydroxybenzylideneimino)-2,3-butenedinitrile ion (L^{2-}) can't stabilize high oxidation state of iron very well. 2) L^{2-} coordinates through two nitrogen atoms and two oxygen atoms to the iron centre, leaving one Cl^- ion and water molecule in *trans* position. This observation strongly suggests that the presence of the Cl^- ion in axial position is the key structural feature for eliciting water oxidation catalysis. [41,42]

Water oxidation occurs at an overpotential of 677 mV, based on the half-peak potential for CVs at pH 10.5 and the reversible potential for $4e^- + O_2 + 4H^+ = 2H_2O$ of 0.61 V at this pH. This overpotential is comparable to the reported homogeneous water-oxidation catalysts (600–900 mV). [43,44]

To prove complex **1** as a homogeneous electrocatalyst, we obtained dependence of the catalytic current on complex **1** concentration. From Fig. S15, the observation of the catalytic current being dependent of **1** concentration could indicate a homogeneous catalyst. And several pieces of evidence also suggest that this complex is a homogeneous catalyst: 1) There is no evidence for a heterogeneous electrocatalytic deposit. For example, the electrode was rinsed with water and electrolysis at -1.45 V vs Ag/AgCl was run for an additional 2 min in a 0.25 M buffer at pH 7.0 with no catalyst present in solution. During this period, ca. 30 mC of charge was passed, a similar magnitude as is observed for electrolysis conducted with freshly polished electrode. 2) At a glass carbon or an ITO electrode, there was no evidence for precipitation formation by ICP (Fig. S16 and Fig. S17) after a 4 h electrolysis period.

Experimental

Elemental analyses for C, H, and N were obtained on a Perkin-Elmer analyzer model 240. UV-Vis spectra were measured on a Hitachi U-3010 spectrophotometer. Cyclic voltammograms were obtained on a CHI-660E electrochemical analyzer under N_2 using a three-electrode cell in which a glassy carbon electrode (1.0 mm in diameter) was the working electrode, a saturated $Ag/AgNO_3$ or Ag/AgCl electrode was the reference electrode, and platinum wire was the auxiliary electrode. In DMF, 0.10 M $[(n\text{-}Bu)_4N]ClO_4$ was used as the supporting electrolyte, and a ferrocene/ferrocenium (1+) couple was used as an internal standard. Controlled-potential electrolysis (CPE) in aqueous media was conducted using an air-tight glass double compartment cell separated by a glass frit. The working compartment was fitted with a glassy carbon plate or an ITO plate and an Ag/AgCl reference electrode. The auxiliary compartment was fitted with a Pt gauze electrode. The working compartment was filled with 50 mL of 0.25 M phosphate buffer solution at different pH values, while the auxiliary compartment was filled with 35 mL phosphate buffer solution. Adding iron complex, the cyclic voltammogram was recorded. After electrolysis, a 0.50 mL aliquot of the headspace was removed and replaced with 0.50 mL of CH_4. A sample of the headspace was injected into the gas chromatograph (GC). GC experiments were carried out with an Agilent Technologies 7890A gas chromatography instrument.

To a solution, containing 2,3-bis(2-hydroxybenzylideneimino)-2,3-butenedinitrile (H_2L) (0.948 g, 3.0 mmol) and triethylamine (0.600 g, 6.0 mmol) in methanol (30 ml), $FeCl_3$ (0.487 g, 3.0 mmol) was added and the mixture was stirred for 15 min. The solution was allowed to slowly evaporate, affording brown crystals, which were collected and dried in *vacuo* (0.877 g, 69%). Calcd for $C_{18}H_{12}ClFeN_4O_3$: C, 50.99; H, 2.83; N, 13.22. Found: C, 50.29; H, 2.85; N, 13.31. UV-vis [CH_3CN, λ_{max}/nm (ε/mol^{-1} cm^{-1})]: 311 (2.46×10^3), 362 (2.12×10^3), 493 (9.46×10^2).

Data was collected with a Bruker SMART CCD area detector using graphite monochromated Mo-Kα radiation (0.71073 Å) at room temperature. All empirical absorption corrections were applied by using the SADABS program. [45] The structures were solved using direct methods and the corresponding non-hydrogen atoms were refined anisotropically. All the hydrogen atoms of the ligands were

placed in calculated positions with fixed isotropic thermal parameters and included in the structure factor calculations in the final stage of full-matrix least-squares refinement. Structure solution and refinement were performed using SHELXTL program. [46] Table S1 lists details of the crystal parameters, data collection and refinement for **1**. The selected bond distances and angles are listed in Table S2.

Conclusions

A new iron(III) complex **1**, which is very easy to be obtained, can electrocatalyze both water reduction water oxidation. **1** electrocatalyzes hydrogen evolution both from acetic acid and purely water media with a TOF of 10.25 (DMF) and 808.46 (buffer, pH 7.0) moles of hydrogen per mole of catalyst per hour, respectively. **1** can also catalyze water oxidation to give O_2 with a TOF of ~0.849 s^{-1} at an overpotential of 677 mV. Our ongoing efforts are focused on modifying ligands to give related water-soluble complexes for further functional studies, with an emphasis on chemistry relevant to sustainable energy cycles.

Acknowledgements

This work was supported by the National Science Foundation of China (No. 20971045 and 21271073), and the Student Research Program (SRP) of South China University of Technology.

Notes and references

College of Chemistry and Chemical Engineering, South China University of Technology, Guangzhou 510640, China. E-mail: shzhzhan@scut.edu.cn.

† Electronic Supplementary Information (ESI) available: CCDC 950008 contains the supplementary crystallographic data for this paper can be obtained free of charge via http://www.ccdc.cam.ac.uk/conts/retrieving.html Experimental section and the synthesis of complexes in this paper are included in the supporting information. See DOI: 10.1039/c000000x/

1 S. Y. Reece, J. A. Hamel, K. Sung, T. D. Jarvi, A. J. Esswein, J. J. H. Pijpers and D. G. Nocera, *Science* 2011, **334**, 645-648.

2 Y. Gao, X. Ding, J. Liu, L. Wang, Z. Lu, L. Li and L. Sun, *J. Am. Chem. Soc*., 2013, **135**, 4219-4222.

3 A. Volbeda, M.-H. Charon, C. Piras, E. C. Hatchikian, M. Fery and J. C. Fontecilla-camps, *Nature* 1995, **373**, 580-587.

4 C. J. Pickett and C. Tard, *Chem. Rev*., 2009, **109**, 2245-2274.

5 J. P. Cao, T. Fang, L. Z. Fu, L. L. Zhou and S. Z. Zhan, *Int. J. Hydrogen Energy* 2014, **39**, 10980–10986.

6 Y. Sun, J. P. Bigi, N. A. Piro, M. L. Tang, J. R. Long and C. J. Chang, *J. Am. Chem. Soc*., 2011, **133**, 9212-9215.

7 B. D. Stubbert, J. C. Peters and H. B. Gray, *J. Am. Chem. Soc*., 2011, **133**, 18070–18073.

8 W. M. Singh, T. Baine, S. Kudo, S. Tian, X. A. N. Ma, H. Zhou, N. J. DeYonker, T. C. Pham, J. C. Bollinger, D. L. Baker, B. Yan, C. E. Webster and X. Zhao, *Angew. Chem. Int. Ed*., 2012, **51**, 5941-5944.

9 L. Z. Fu, L. L. Zhou, L. Z. Tang, Y. X. Zhang and S. Z. Zhan, *J. Power Sources* 2015, **280**, 453-458.

10 L. L. Zhou, L. Z. Fu, L. Z. Tang, Y. X. Zhang and S. Z. Zhan, *Int. J. Hydrogen Energy* 2015, **4 0**, 5 0 9 9 -5 1 0 5.

11 J. P. Cao, T. Fang, L. Z. Fu, L. L. Zhou and S. Z. Zhan, *Int. J. Hydrogen Energy* 2014, **39**, 13972-13978.

12 J. P. Cao, T. Fang, Z. Q. Wang, Y. W. Ren and S. Z. Zhan, *J. Mol. Cata. A: Chem*., 2014, **391**, 191–197.

13 L. L. Zhou, T. Fang, J. P. Cao, Z. H. Zhu, X. T. Su and S. Z. Zhan, *J. Power Sources* 2015, **273**, 298-304.

14 L.-Z. Fu, T. Fang, L.-L. Zhou and S.-Z. Zhan, *RSC. Adv*., 2014, **4**, 53674-53680.

15 H. I. Karunadasa, C. J. Chang and J. R. Long, *Nature* 2010, **464**, 1329-1333.

16 J. P. Cao, T. Fang, L. L. Zhou, L. Z. Fu and S. Z. Zhan, *Electrochimica Acta* 2014, **147**, 129-135.

17 J. P. Cao, L. L. Zhou, L. Z. Fu and S. Z. Zhan, *J. Power Sources* 2014, **272**, 169-175.

18 Q. Yin, J. M. Tan, C. Besson, Y. V. Geletii, D. G. Musaev, A. E. Kuznetsov, Z. Luo, K. I. Hardcastle and C. L. Hill, *Science* 2010, **328**, 342–345.

19 D. K. Dogutan, R. McGuire and D. G. Nocera, *J. Am. Chem. Soc*., 2011, **133**, 9178–9180.

20 D. J. Wasylenko, C. Ganesamoorthy, J. Borau-Garcia and C. P. Berlinguette, *Chem. Commun*., 2011, **47**, 4249-4251.

21 S. M. Barnett, K. I. Goldberg and J. M. Mayer, *Nat. Chem*., 2012, **4**, 498-502.

22 T. Zhang, C. Wang, S. Liu, J. Wang and W. Lin, *J. Am. Chem. Soc*., 2014, **136**, 273–281.

23 J. Lloret-Fillol, Z. Codol, I. Garcia-Bosch, L. Gmez, J. J. Pla and M. Costas, *Nat. Chem*., 2011, **3**, 807–813.

24 M. Z. Ertem, L. Gagliardi and C. J. Cramer, *Chem. Sci*., 2012, **3**, 1293–1299.

25 R. Sarma, A. M. Angeles-Boza, D. W. Brinkley and J. P. Roth, *J. Am. Chem. Soc*., 2012, **134**, 15371–15386.

26 D. Hong, Y. Yamada, T. Nagatomi, Y. Takai and S. Fukuzumi, *J. Am. Chem. Soc*., 2012, **134**, 19572–19575.

27 G. Chen, L. Chen, S. Ng, W. Man and T. Lau, *Angew. Chem. Int. Ed*., 2013, **52**, 1789–1791.

28 M. K. Coggins, M. Zhang, A. K. Vannucci, C. J. Dares and T. J. Meyer, *J. Am. Chem. Soc*., 2014, **136**, 5531–5534.

29 Q. Yin, J. M. Tan, C. Besson, Y. V. Geletii, D. G. Musaev, A. E. Kuznetsov, Z. Luo, K. I. Hardcastle and C. L. Hill, *Science* 2010, **328**, 342–345.

30 J. L. Dempsey, B. S. Brunschwig, J. R. Winkler and H. B. Gray, *Acc. Chem. Res*., 2009, **42**, 1995–2004.

31 U. Koelle and S. Ohst, *Inorg. Chem*., 1986, **25**, 2689–2694.

32 L. L. Zhou, T. Fang, J. P. Cao, Z. Zhu, X. Su and S. Z. Zhan, *J. Power Sources* 2015, **273**, 298-304.

33 R. Viswanathan, M. Palaniandavar, T. Balasubramanian and T. P. Muthiah, *Inorg. Chem.,* 1998, **37**, 2943-2951.

34 M. K. Coggins, M. Zhang, A. K. Vannucci, C. J. Dares and T. J. Meyer, *J. Am. Chem. Soc*., 2014, **136**, 5531-5534.

35 M. R. Norris, J. J. Concepcion, D. P. Harrison, R. A. Binstead, D. L. Ashford, Z. Fang, J. L. Templeton and T. J. Meyer, *J. Am. Chem. Soc*., 2013, **135**, 2080−2083.

36 Z. Chen, J. J. Concepcion, H. Luo, J. F. Hull, A. Paul and T. J. Meyer, *J. Am. Chem. Soc*., 2010, **132**, 17670−17673.

37 J. F. Hull, D. Balcells, J. D. Blakemore, C. D. Incarvito, O. Eisenstein, G. W. Brudvig and R. H. Crabtree, *J. Am. Chem. Soc*., 2009, **131**, 8730-8731.

38 W. C. Ellis, N. D. McDaniel, S. Bernhard and T. J. Collins, *J. Am. Chem. Soc*., 2010, **132**, 10990-10991.

39 J. Concepcion, J. Jurss, P. Hoertz and T. Meyer, *Angew. Chem. Int. Ed*., 2009, **48**, 9473-9476.

40 Z. Q. Wang, Z. C. Wang, S. Z. Zhan and J. S. Ye, *Applied Catalysis A: Gerenal* 2015, **490**, 128-132.

41 J. J. Concepcion, M. Tsai, J. T. Muckerman and T. J. Meyer, *J. Am. Chem. Soc*., 2010, **132**, 1545-1557.

42 K. S. Joya, N. K. Subbaiyan, F. D'Souza and H. J. M. de Groot, *Angew. Chem., Int. Ed*., 2012, **51**, 9601−9605.

43 J. J. Concepcion, J. W. Jurss, M. K. Brennaman, P. G. Hoertz, A. O. T. Patrocinio, N. Y. M. Iha, J. L. Templeton and T. J. Meyer, *Acc. Chem. Res*., 2009, **42**, 1954–1965.

44 J. G. McAlpin, T. A. Stich, C. A. Ohlin, Y. Surendranath, D. G. Nocera, W. H. Casey and R. D. Britt, *J. Am. Chem. Soc*., 2011, **133**, 15444–15452.

45 G. M. Sheldrick, SADABS, Program for Empirical Absorption Correction of Area Detector Data, University of Götingen, Götingen, Germany, (1996)

46 G. M. Sheldrick, SHELXS 97, Program for Crystal Structure Refinement, University of Götingen, Götingen, Germany, (1997)

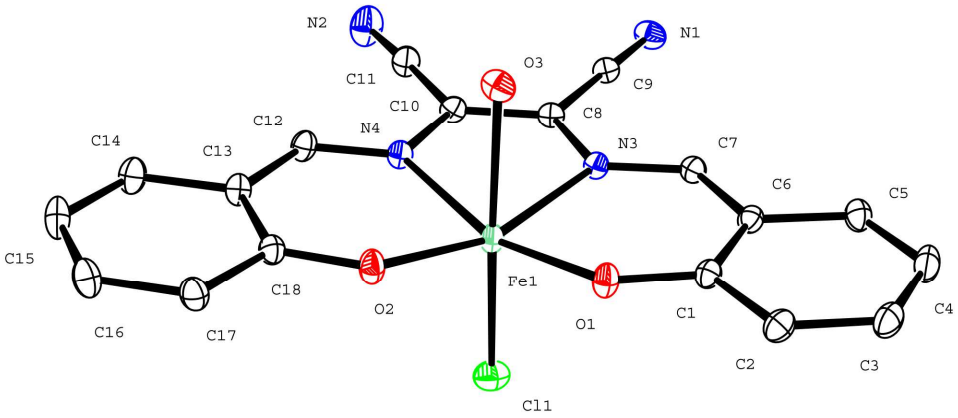

Fig. 1. X-ray structure of complex **1**

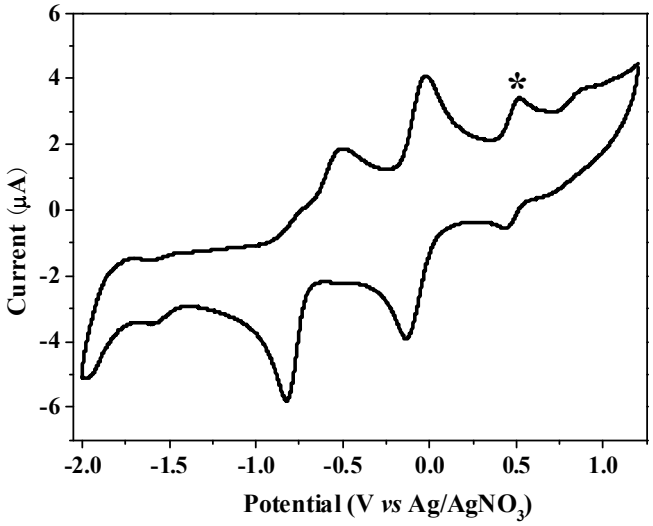

Fig. 2. Cyclic voltammogram of 3.17 mM complex **1** in 0.10 M of [n-Bu_4N]ClO_4 DMF solution at a glassy carbon electrode and a scan rate of 100 mV/s. Ferrocene internal standard (*).

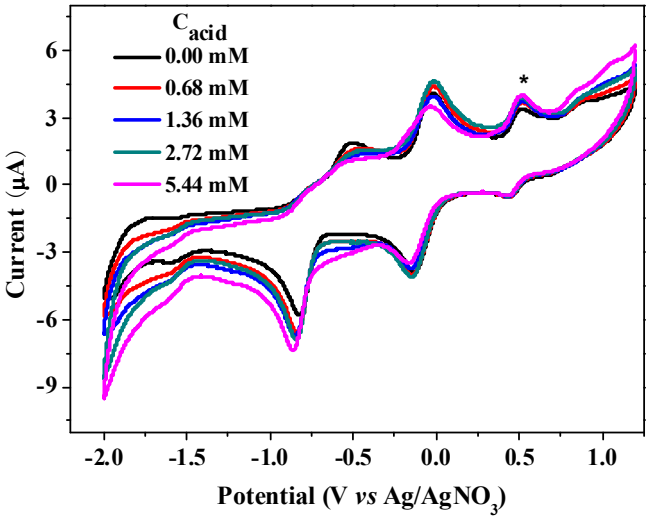

Fig. 3. Cyclic voltammograms of a 3.17 mM solution of complex **1**, with varying concentrations of acetic acid in DMF. Conditions: 0.10 M $[n\text{-}Bu_4N]ClO_4$ as supporting electrolyte, scan rate: 100 mV/s, GC working electrode (1 mm diameter), Pt counter electrode, $Ag/AgNO_3$ reference electrode, Fc internal standard (*).

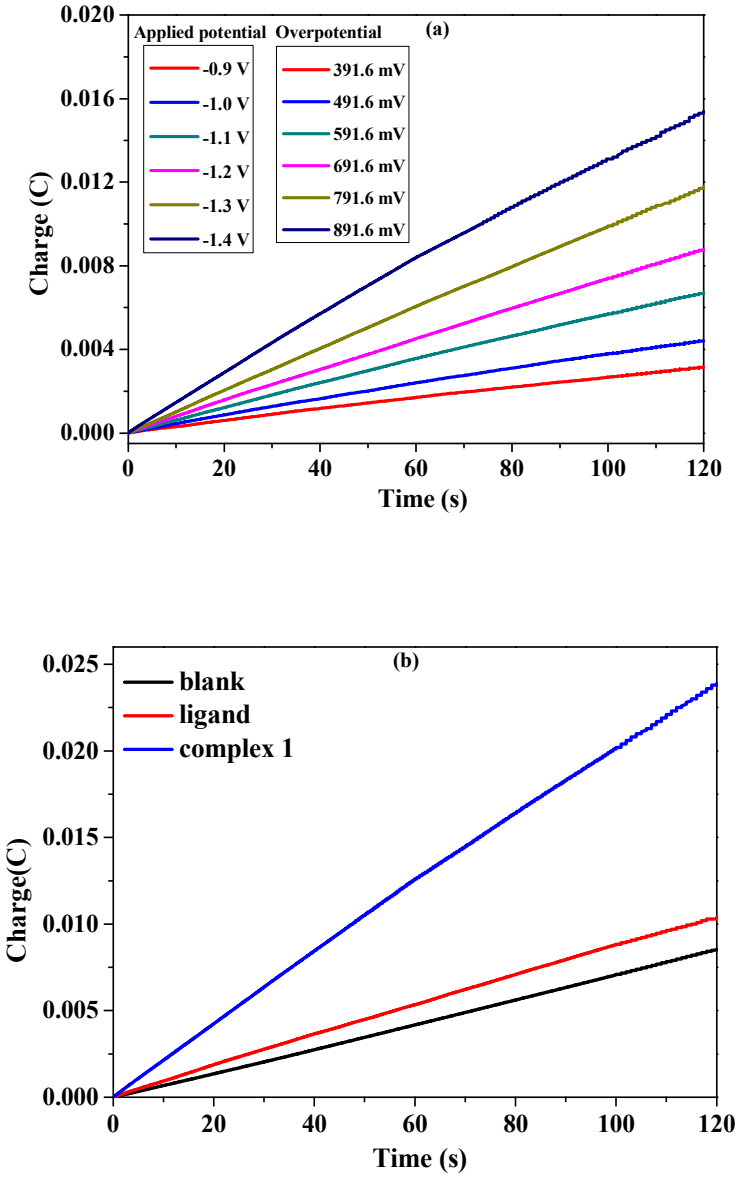

Fig. 4. (a) Charge buildup versus time from electrolysis of 5.44 mM CH_3COOH in DMF (0.10 M [n-Bu_4N]ClO_4) with 5.80 μM complex **1** under various applied potentials. All data have been deducted blank. (b) Charge buildup versus time from electrolysis of a 5.44 mM CH_3COOH DMF solution (0.10 M [n-Bu_4N]ClO_4) (black), with 5.80 μM ligand (red) and 5.80 μM complex **1** (blue) under -1.40 V *vs* $Ag/AgNO_3$.

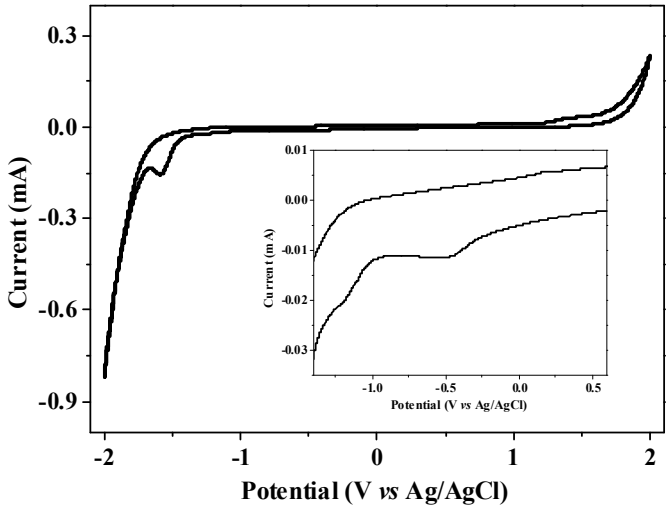

Fig. 5. Cyclic voltammogram of complex **1** (1.71 mM) in a 0.25 M phosphate buffered solution of pH 7.0 at GC working electrode (1.0 mm diameter), Pt wire counter electrode, Ag/AgCl reference electrode. The inset shows a magnified view of the Fe^{III}/Fe^{II} couple.

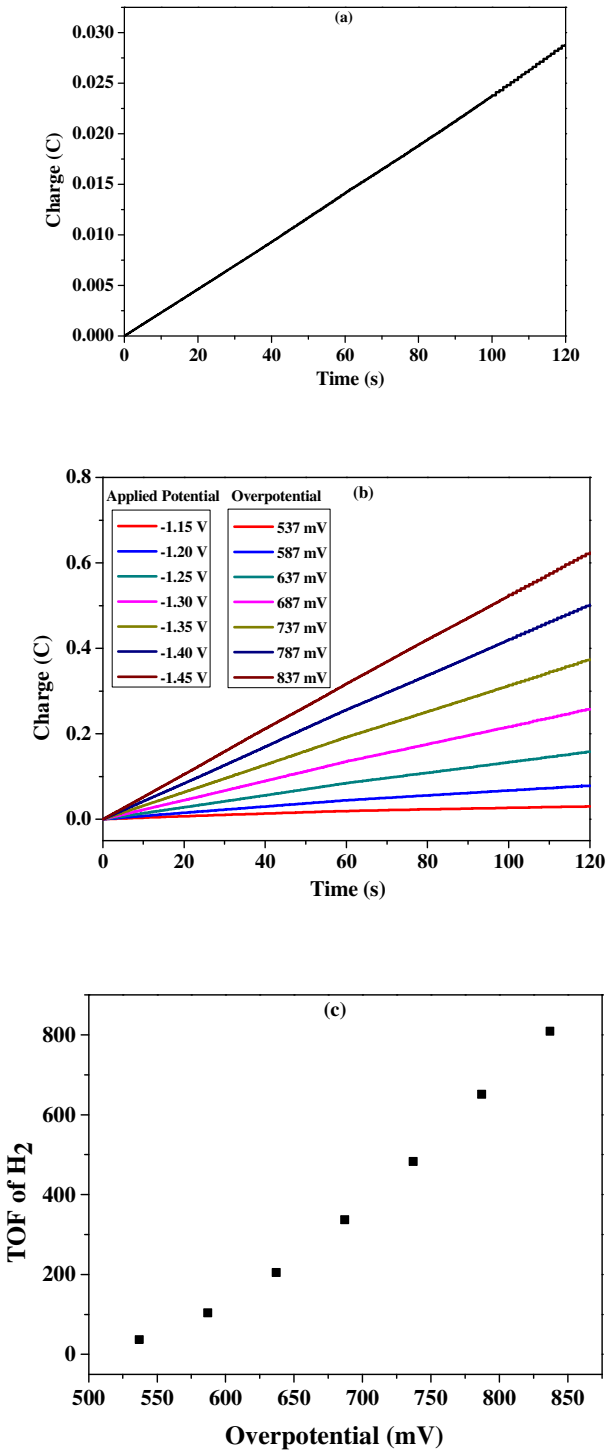

Fig. 6. (a) Charge buildup of buffer (pH 7.0). (b) Charge buildup of complex **1** (0.12 μM) versus a series of applied potentials in 0.25 M buffer at pH 7.0. All data have been deducted blank. (c) Turnover frequency (mol H_2/mol catalysts/h) for electrocatalystic hydrogen production by complex **1** (0.12 μM) under overpotentials.

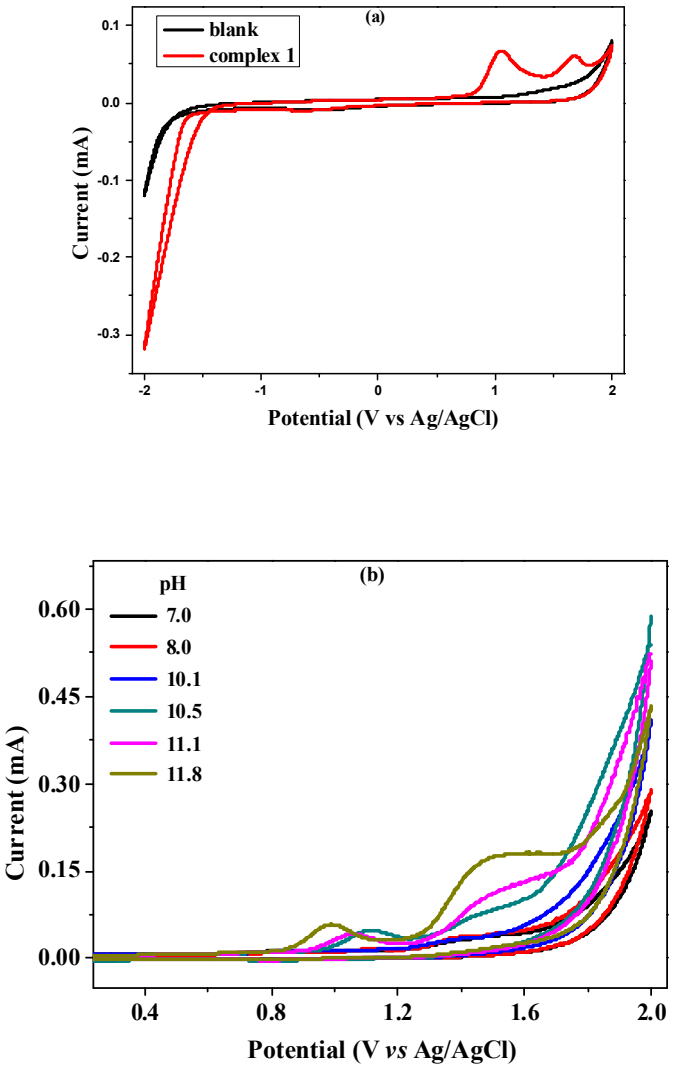

Fig. 7. (a) Cyclic voltammogram of complex **1** (1.71 mM) in 0.10 M KNO_3 at a glassy carbon electrode and a scan rate of 100 mV/s. (b) Cyclic voltammograms of complex **1** (1.71 mM) in buffers (KH_2PO_4 + NaOH) at different pHs.

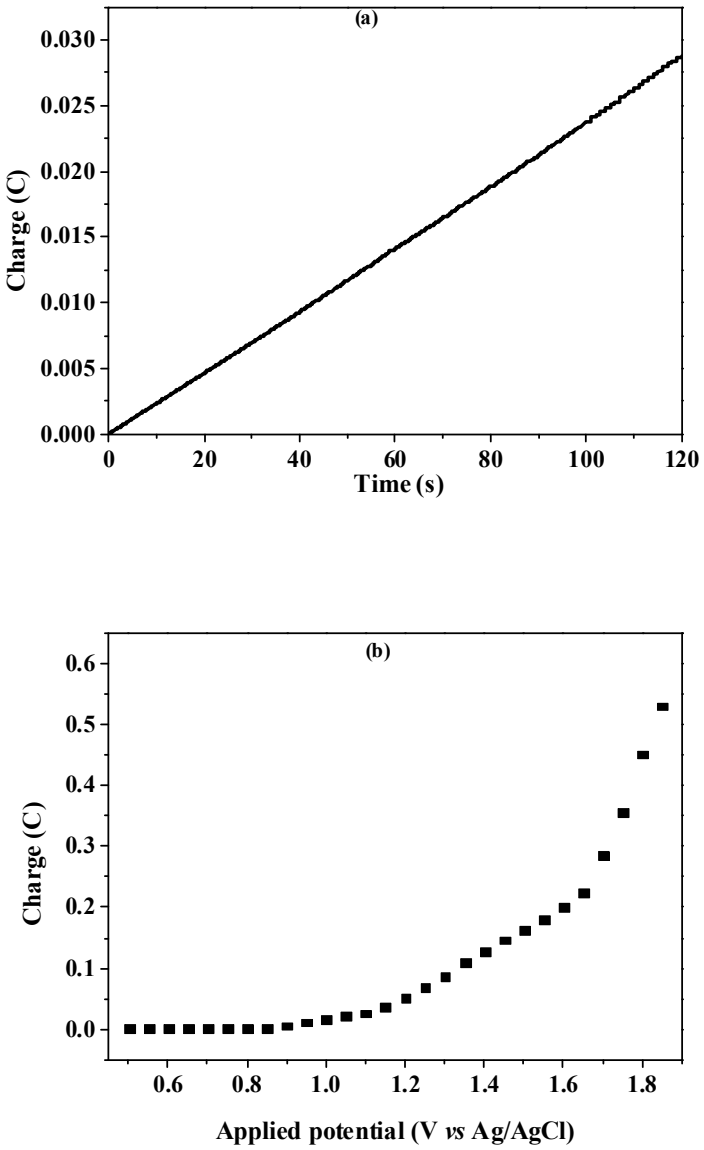

Fig. 8. (a) Charge buildup of a 0.25 M buffer (KH_2PO_4 + NaOH) at pH 10.5. (b) Charge buildup versus a series of applied potentials by a 17.4 μM complex **1** in 0.25 M buffer (KH_2PO_4 + NaOH) at pH 10.5. All data have been deducted blank.

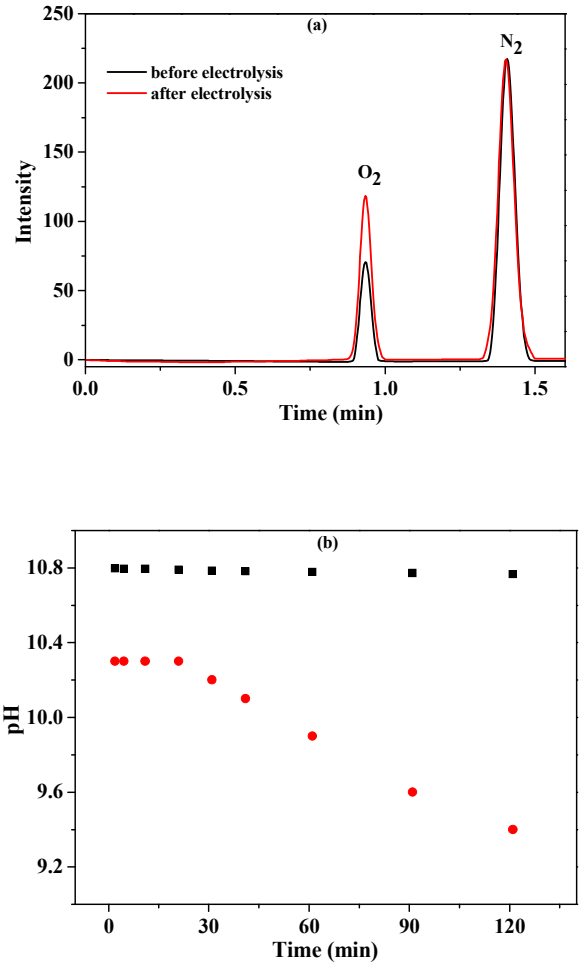

Fig. 9. (a) GC traces after a 5-h controlled-potential electrolysis at 1.45 V Ag/AgCl of 15.93 μM complex **1** in 0.25 M buffer (KH_2PO_4 + NaOH), pH 10.5. (b) Measured (red) and calculated (black) pH changes assuming a 100% Faradic efficiency of complex **1** during electrolysis. (the theoretical pH change over time can be calculated by the equation of $pH = 14 + \lg\frac{\sum It}{FV}$ where I = current (A), t = time (s), F = Faraday constant (96485 C/mol), V = solution volume (0.04 L)).